Journal of Atmospheric and Solar-Terrestrial Physics 71 (2009) 1592–1601

Contents lists available at ScienceDirect

Journal of Atmospheric and Solar-Terrestrial Physics

journal homepage: www.elsevier.com/locate/jastp

The effect of carbon dioxide cooling on trends in the F2-layer ionosphere

Liying Qian *, Alan G. Burns, Stanley C. Solomon, Raymond G. Roble

High Altitude Observatory, National Center for Atmospheric Research, 3080 Center Green Drive, Boulder, CO 80301, USA

ARTICLE INFO

Article history:
Accepted 8 March 2009
Available online 20 March 2009

Keywords:
Ionospheric trends
Greenhouse effect
Photochemical forcing
Dynamical forcing
Composition (O/N_2)
Plasma transport

ABSTRACT

The effect of carbon dioxide (CO_2) cooling on trends of h_mF_2 and N_mF_2 are investigated using a coupled thermosphere and ionosphere general circulation model. Model simulations indicate that CO_2 cooling not only causes contraction of the upper atmosphere and changes of neutral and ion composition but also changes dynamics and electrodynamics in the thermosphere/ionosphere. These changes determine the altitude dependence of ionospheric trends and complex latitudinal, longitudinal, diurnal, seasonal, and solar cycle variations of trends of h_mF_2 and N_mF_2. Under the CO_2 cooling effect, trends of N_mF_2 are negative with magnitude from 0% to ~−40% for doubled CO_2, depending on location, local time, season, and solar activity. The corresponding trends of h_mF_2 are mostly negative with a magnitude from 0 to −40 km, but can be positive with a magnitude from 0 to ~10 km at night, with maximum positive trends occurring after midnight under solar minimum conditions.

1. Introduction

Long-term changes in the upper atmosphere and ionosphere have been of great interest since Roble and Dickinson (1989) suggested that global cooling will occur in the upper atmosphere in conjunction with global warming in the troposphere due to long-term increase of greenhouse gas concentrations, particularly carbon dioxide (CO_2). This cooling is caused by collision-induced infrared radiation by CO_2 and other heterogenous molecules as the atmosphere above the tropopause becomes increasingly transparent to infrared radiation. Thus, instead of causing warming as in the troposphere, the "greenhouse effect" in the upper atmosphere reduces temperature and causes the thermosphere to contract, reducing its density as a function of altitude. This has practical importance due to its influence on satellite drag. In addition, determination of long-term changes in the upper atmosphere and ionosphere has important scientific interest. It can facilitate understanding of global change in the lower atmosphere since global change in the lower atmosphere and upper atmosphere/ionosphere are closely linked, and it can be easier to detect global changes in the upper atmosphere and ionosphere due to larger signal to noise ratio (Laštovička et al., 2006a). Significant progress has been made after nearly two decades of observational and modeling studies (e.g., Akmaev and Fomichev, 1998, 2000; Akmaev et al., 2006; Beig, et al., 2003; Bremer et al., 2004; Clilverd et al, 2003; Danilov and Mikhailov, 1999; Emmert et al., 2004; Gruzdev and Brasseur, 2005; Keating et al., 2000; Laštovička and Bremer, 2004; Laštovička, 2005; Laštovička et al., 2008; Marcos et al., 2005; Mikhailov and Marin, 2000, 2001; Qian et al., 2006, 2008; Rishbeth, 1990, 1997; Rishbeth and Roble, 1992; Xu et al., 2004). Consistent results have been obtained regarding long-term trends of mesospheric temperature, electron density in the lower ionosphere and F_1-region, *hmE* and *NmE*, and thermospheric neutral density (Laštovička et al., 2006a, 2008). These results support the hypothesis of cooling and contraction of the upper atmosphere as a result of increased greenhouse gas concentrations.

However, controversies and discrepancies remain for detection of trends of F_2 peak parameters (h_mF_2 and N_mF_2), regarding methods of data analysis, the magnitudes of the trends, and interpretation of the causes of the trends. Since these trends of h_mF_2 and N_mF_2 are relatively weak compared to the strong natural variability due to solar and geomagnetic activity, different analysis methods resulted in discrepancies of more than one order of magnitude (Laštovička et al., 2006b). There are two interpretations of the cause of these trends of h_mF_2 and N_mF_2: geomagnetic origin and greenhouse gas cooling effects. Mikhailov et al. (2002) found a small negative residual trend of foF_2 with a natural origin related to long-term variations in solar and geomagnetic activity, but no indication of any manmade effects. Mikhailov (2006) further indicated that thermosphere cooling due to the greenhouse gases is not noticeable in the foF_2 trends due to the weak dependence of N_mF_2 on neutral temperature and, therefore, foF_2 trends are completely controlled by long-term variations of geomagnetic activity. On the other hand, Bremer (1992) found a negative trend in h_mF_2 for a mid-latitude station over time; this supports global cooling of the thermosphere due to greenhouse

* Corresponding author. Tel.: +1 303 497 1529; fax: +1 303 497 2180.
E-mail address: lqian@ucar.edu (L. Qian).

1364-6826/$ - see front matter © 2009 Elsevier Ltd. All rights reserved.
doi:10.1016/j.jastp.2009.03.006

gases. Danilov (2002) developed a method of determining of long-term trends of non-geomagnetic origin, and found a negative trend in foF_2 for the period 1958–1995, which is substantially larger than that for the period of 1948–1985, which supports its anthropogenic origin. Attempts were also made to reconcile the greenhouse and geomagnetic activity causes of these trends. It was suggested that there is simultaneous greenhouse control of the trend in h_mF_2 and geomagnetic control of the trend in foF_2 (e.g., Mikhailov, 2006).

In addition, trends of F_2 peak parameters exhibit variations with geographic location, local time, season, and solar activity. Controversies exist regarding these variations. Bremer (1998, 2001) obtained h_mF_2 and foF_2 trends of different signs for 31 European stations, with negative trends west of 30°E but positive trends east of 30°E. He suggested that trends of F_2 parameters cannot be explained by the increasing greenhouse effect alone and that dynamical effects seem to play an important role. Danilov and Mikhailov (1999) found negative trends for all individual stations they selected, and detected a strong and well pronounced dependence of the foF_2 trends on geomagnetic latitude but no longitudinal dependence, which is contrary to Bremer's finding (1998, 2001). Mikhailov and Marin (2000) found diurnal variations of foF_2 trends, with foF_2 having its minimum trend at local noon and its maximum at night. Danilov (2008) found long-term variations in the relation between daytime and nighttime foF_2 and evoked long-term variations of thermospheric meridional wind to explain these variations. Furthermore, variability in trends of F_2 peak parameters has also been used as evidence of the origin of these trends. Mikhailov and Marin (2000, 2001) and Mikhailov et al. (2002) argued that trends of foF_2 due to greenhouse gas cooling should be positive and should not have complex latitudinal, longitudinal, and diurnal variations, and that latitudinal and diurnal variations of foF_2 trends are evidence of geomagnetic control of the foF_2 trend.

So what are the signs and magnitudes of trends of the F_2 peak parameters and what has been causing their long-term trends? It is likely that both natural trends of solar and geomagnetic activity and anthropogenic trends through the greenhouse gas cooling effect have contributed to long-term trends of the F_2 peak parameters. It is important to understand how the trends of the F_2 peak parameters are influenced by each forcing process in order to determine contributions from each forcing type and identify the driving mechanisms of these trends. In data analysis, it is difficult to separate contributions from forcing of natural origin and the greenhouse effect. For example, it is difficult to explain the origin of complex features of trend dependence on geographic location, local time, season, and solar activity. Modeling studies can be a great tool to separate contributions from the two forcing types and to understand the distribution of trends with location and variations with local time, season, and solar activity. Furthermore, possible dynamic influences on trends of F_2 peak parameters has been speculated about and used to explain the observed features of trend variations (e.g., Bremer, 1998; Danilov, 2008). In this paper we will use a three-dimensional general circulation model to examine dynamic influences on these trends.

Qian et al. (2008) used a one-dimensional model to investigate trends in the global mean ionosphere. In this paper, we will use a three-dimensional upper atmospheric general circulation model to investigate how the three-dimensional ionosphere, particularly foF_2 and h_mF_2, responds to increased CO_2 concentrations in the atmosphere. Specifically, the model will be used to examine the geographic pattern of these trends, their diurnal and seasonal variations, and the dependence of these trends on solar activity. The model will also be used to determine dynamical influences on trends and their variability. Section 2 describes the three-dimensional upper atmosphere general circulation model; Section 3 shows model simulation results; Section 4 provides some discussion; and Section 5 concludes the study.

2. Model description

The model used for this study is the National Center for Atmospheric Research (NCAR) Thermosphere–Ionosphere-Electrodynamic General Circulation Model (TIEGCM). The TIEGCM is a first-principles numerical model that solves the Eulerian continuity, momentum, and energy equations for the coupled thermosphere/ionosphere system (Dickinson et al., 1981, 1984; Roble and Ridley, 1987; Roble et al., 1988; Richmond et al., 1992; Richmond, 1995). It utilizes a spherical coordinate system fixed with respect to the rotating Earth, with latitude and longitude as the horizontal coordinates and pressure surfaces as the vertical coordinate. The pressure interfaces are defined as $z = \ln(P_0/P)$, where P_0 is a reference pressure of 5×10^{-4} μb. The vertical range of these pressure surfaces is from -7 to 7, and thus covers an altitude range of about 97–600 km, depending on solar activity. The vertical resolution is 2 model grids per pressure scale height; the horizontal resolution is 5° latitude by 5° longitude, and the model time step is about 3 min. Output of the model are neutral, electron, and ion temperatures; neutral and ion winds; concentrations of major species O, O_2, and N_2; concentrations of minor species N(^{4}S), N(^{2}D), NO; concentrations of ions O^+,O_2^+, N_2^+, N^+, NO^+; electron density; and geopotential heights of pressure interfaces.

The external forcing of the TIEGCM are solar irradiance, mainly in the extreme ultraviolet (EUV) and ultraviolet (UV) regions; geomagnetic energy input in the form of auroral energetic particle precipitation and ionospheric convection driven by the magnetosphere–ionosphere current system; perturbation at the lower boundary of the model by waves representing the interaction between the thermosphere/ionosphere system and lower atmosphere processes; and a specified upward or downward plasma flux at the upper boundary representing the interaction of the system with the plasmasphere. In this study, the EUVAC solar proxy model (Richards et al., 1994) was used as solar input. Ionospheric convection driven by the magnetosphere–ionosphere current system is specified by the empirical model of Heelis et al. (1982). Auroral particle precipitation and its ionization and dissociation are calculated by an analytical auroral model described by Roble and Ridley (1987). The migrating semi-diurnal and diurnal tides are specified at the lower boundary using the Global Scale Wave Model (GSWM) (Hagan and Forbes, 2002, 2003). The effect of gravity wave breaking in the mesosphere–lower-thermosphere (MLT) region is included by specifying eddy diffusivity at the lower boundary that declines with altitude. Effects of planetary waves and non-migrating tides are not considered.

Since the goal of this paper is to examine and separate contribution of the greenhouse gas cooling effect on the global distribution of ionospheric trends, we conducted all model runs under geomagnetic quiet conditions. Since CO_2 is the main cooler of the upper atmosphere, we consider the effect of changes of CO_2 concentrations. Changes of other radiatively active gases, such as stratospheric ozone depletion and possible stratospheric and mesospheric water vapor increases, may also slightly affect long-term changes of the ionosphere since Akmaev et al. (2006) have demonstrated the effects of ozone depletion and water vapor increase on lower thermospheric temperature and density. However, this secondary effect is not treated here. The model was run with base (365 ppmv) and doubled CO_2 concentrations (730 ppmv), for both solar minimum and solar maximum, near the June solstice. The 365 ppmv characterizes present-day CO_2

concentration while 730 ppmv represents a projection of CO_2 concentration for year 2100 by the Intergovernmental Panel on Climate Change (IPCC) (2007) emission scenario A1B, a medium emission scenario. These CO_2 concentrations were applied at the model lower boundary. Above the lower boundary, CO_2 concentrations decrease exponentially with pressure scale height.

3. Results

Ionosonde data analysis indicated that trends of foF_2 and h_mF_2 vary with geographic location, local time, and season (e.g. Bremer, 1998; Mikhailov and Marin, 2000; Xu et al., 2004; Danilov, 2008). In addition, solar activity influence on ionospheric trend detection is evident (Clilverd et al., 2003). The TIEGCM model was run with base and doubled CO_2 concentrations, for both solar minimum and solar maximum, under geomagnetic quiet condition, and near June solstice to include these possible variations. These model runs were designed to investigate the geographic distribution of ionospheric trends, diurnal and seasonal variations of possible trends, and the effect of solar activity on trends, under the CO_2 cooling effect. Changes of h_mF_2 and N_mF_2 due to increased CO_2 concentrations were calculated and shown for different local times (longitude as the *X*-axis and latitude as the *Y*-axis), for both solar minimum and solar maximum conditions. Since the model uses pressure surfaces as the vertical coordinate and thus solves the continuity, momentum, and energy equations on pressure surfaces, least-square second-degree polynomial fitting was performed to the model-simulated vertical electron density profiles to obtain h_mF_2 and N_mF_2. Figs. 1 and 2 are results for local time 12:00 noon and 3:00 am, respectively, which show the dependence of F_2 peak trends on geographic location, local time, season, and solar activity. 3:00 am was selected to represent nighttime since it is around the time when positive trends of h_mF_2 are prominent. Changes of h_mF_2 and N_mF_2 shown in Figs. 1 and 2 are absolute changes and percentage changes, respectively. Trends of N_mF_2 are investigated in this paper, but the relationship between N_mF_2 and foF_2 is: $N_mF_2 = 1.24 \times 10^{10}(f_oF_2)^2$, where N_mF_2 is in m^{-3} and foF_2 is in MHz. We will first observe the overall patterns of h_mF_2 and N_mF_2 variations with geographic location, local time, season, and solar activity. We will then examine how photochemical processes and plasma transport control these patterns. Finally, we will briefly look at the vertical distribution of ionospheric trends due to the CO_2 cooling effect.

3.1. Overall trends of h_mF_2 and N_mF_2

Figs. 1 and 2 show that under the CO_2 cooling effect, trends of N_mF_2 are negative. Percentage changes of N_mF_2 range from 0 to ~−40% depending on location, local time, season, and solar activity. The corresponding trends of h_mF_2 are overall negative as well, with a magnitude from 0 to ~−40 km, also depending on location, local time, season, and solar activity. However, trends of h_mF_2 can be positive, usually after midnight, with a maximum positive trend of ~10 km. The following trend variability can be observed from Figs. 1 and 2:

Geographic location (*latitude and longitude*): Trends of h_mF_2 and N_mF_2 exhibit large latitudinal and longitudinal variations in both daytime (Fig. 1) and nighttime (Fig. 2). Both latitudinal and longitudinal distributions of these trends show correlation with the geomagnetic dip equator, indicating the effects of electrodynamics on these trends.

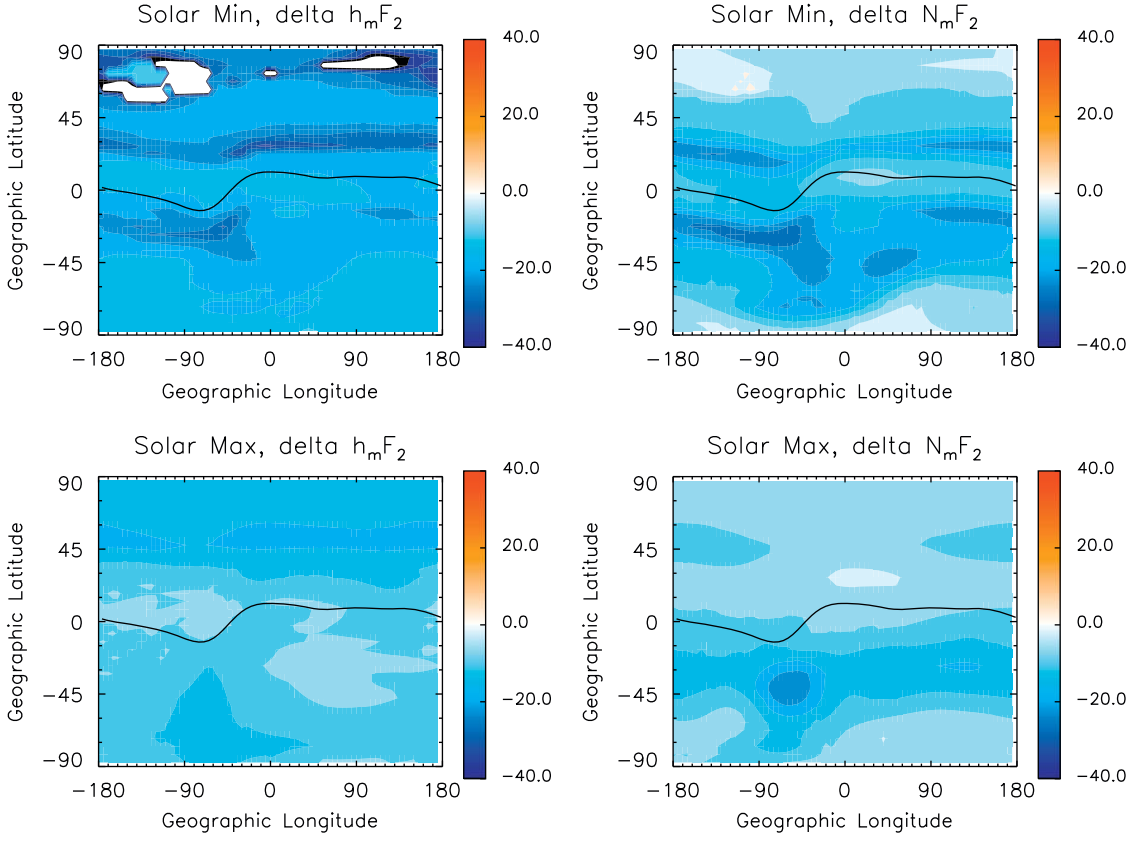

Fig. 1. Changes of h_mF_2 and N_mF_2 (double CO_2–base CO_2) at local noon for solar minimum (upper panels) and solar maximum (lower panel) conditions. Changes of h_mF_2 are absolution changes in km while changes of N_mF_2 are percentage changes. Solar minimum: $F_{10.7} = \overline{F_{10.7}} = 70$; Solar maximum: $F_{10.7} = \overline{F_{10.7}} = 200$. Geomagnetic K_p index is 1, i.e., under geomagnetic quiet condition. The black line in each figure is geomagnetic dip equator.

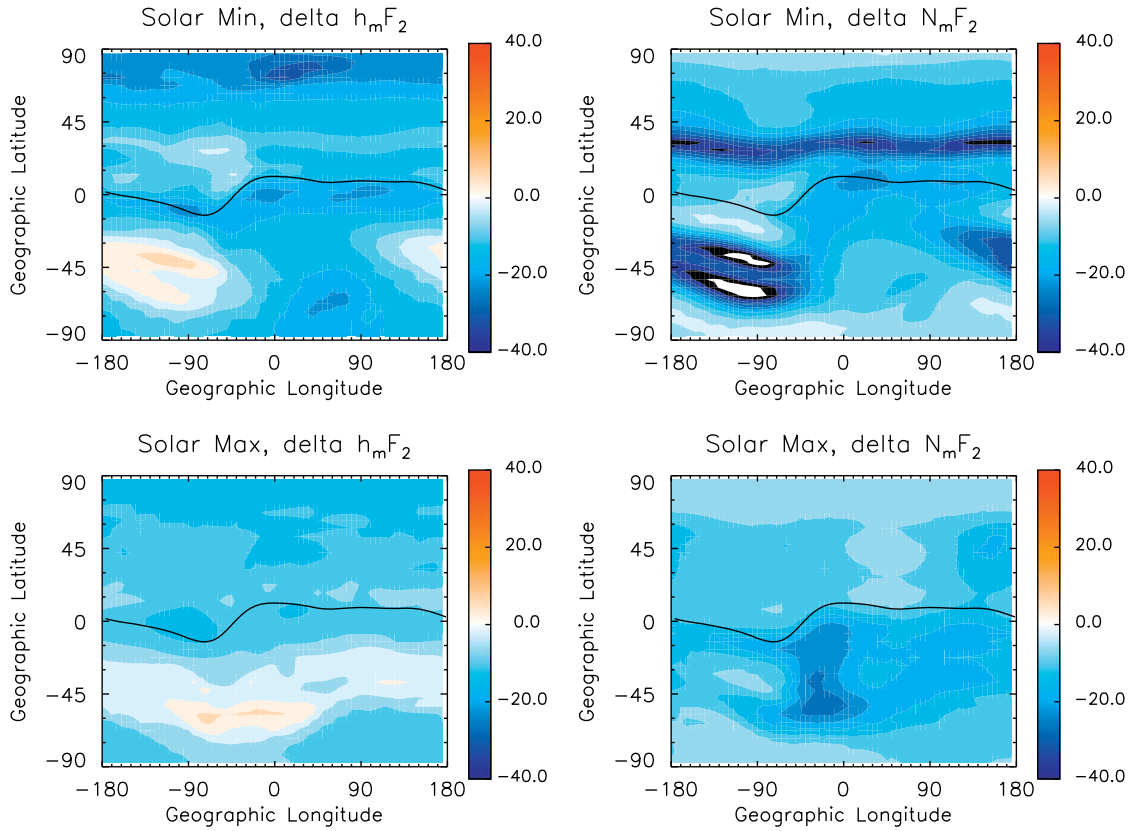

Fig. 2. Changes of h_mF_2 and N_mF_2 (double CO_2–base CO_2) at 3:00 am for solar minimum (upper panels) and solar maximum (lower panel) conditions. Changes of h_mF_2 are absolution changes in km while changes of N_mF_2 are percentage changes. Solar minimum: $F_{10.7} = \overline{F_{10.7}} = 70$; solar maximum: $F_{10.7} = \overline{F_{10.7}} = 200$. Geomagnetic K_p index is 1, i.e., under geomagnetic quiet condition. The black line in each figure is geomagnetic dip equator.

Local time: Figs. 1 and 2 show that trends of h_mF_2 and N_mF_2 have strong local time dependence, and that this local time dependence varies at different geographic locations. Some locations have larger trends during nighttime while other locations have their largest trends during the day. In addition, trends of N_mF_2 are negative over the globe during both the day (Fig. 1) and the night (Fig. 2), whereas trends of h_mF_2 are all negative during the day (Fig. 1), but can be positive at some locations at night (Fig. 2); On average, the trend of N_mF_2 at 3:00 am (Fig. 2) is larger than that at 12:00 noon (Fig. 1), for both solar minimum and solar maximum conditions; Positive h_mF_2 trends at night correspond to where the maximum trend of N_mF_2 occurs, which is in the winter hemisphere.

Season: Trends of F_2 peak parameters show different patterns in the winter and summer hemispheres. Particularly, trends of N_mF_2 are larger in the winter hemisphere than those in the summer hemisphere overall, for both solar minimum and solar maximum conditions.

Solar activity: On a globally average basis, trends of both h_mF_2 and N_mF_2 are larger under solar minimum conditions than under solar maximum conditions, and the global distribution of trends tends to be more structured under solar minimum conditions.

3.2. Analysis of trends of h_mF_2 and N_mF_2

The F_2 peak is the place where the effects of plasma transport processes become comparable to the effects of photochemical processes (Rishbeth, 1998). Below the F_2 peak altitude, photochemical processes control electron density whereas above the F_2 peak, plasma transport controls electron density. Model simulations show that trends of F_2 peak parameters have a distinct global distribution and exhibit variations with local time, season, and solar activity. It is important to understand the roles of photochemical processes and plasma transport in determining trends of F_2 parameters and variability of these trends; and how photochemical processes and plasma transport contribute to the trends and trend variability.

In order to understand the underlying physics of trends and the associated trend features, we need to examine the governing processes that determine electron density and its altitude profile. The ionosphere is approximately under charge neutrality in the *E* and *F* regions, i.e., the electron number density is approximately equal to the sum of the number densities of ions. The TIEGCM obtains electron number density by calculating ion number densities. The major ion at the F_2 peak is O^+. The model solves the following O^+ continuity equation:

$$\frac{\partial n}{\partial t} = Q - Ln + transport \quad (1)$$

where n is O^+ number density, Q is total production of O^+ through ionization by photons and photoelectrons, dissociative ionization by photon and photoelectrons, and chemical reactions; L is the total loss of O^+ through charge exchange and chemical reactions of O^+ with neutrals. The transport term includes plasma transport by ambipolar diffusion, neutral wind, and $\vec{E} \times \vec{B}$ drift. $\vec{E}$ is electric field, which is mainly of magnetospheric-origin at high latitudes, but is largely generated by the neutral wind dynamo at low latitudes; $\vec{B}$ is the Earth's magnetic field.

At the F_2 peak, the main photochemical production of O^+ is photoionization of O ($O+h\nu \rightarrow O^+ + e$). The main photochemical loss is a two-step process, with transfer of O^+ to the molecular ions

NO^+ and O_2^+ through atom–ion interchange reactions ($O^+ + N_2 + N_2 \rightarrow NO^+ + N$, $O^+ + O_2 \rightarrow O_2^+ + O$) followed by dissociative recombination of the two molecular ions. The atom–ion interchange reaction rates are much slower than the dissociative recombination rates. If the F_2 peak is under photochemical equilibrium, then electron density will be approximately determined by the balance between the photoionization rate of O and atom–ion interchange reaction rates, therefore, electron density would be proportional to O/N_2 through balance of these photochemical production and loss processes considering N_2 is the main molecular species at the F_2 peak. However, unlike in the E and F_1 regions, the possible photochemical equilibrium in the F_2 peak is, in practice, modified by plasma transport. Nevertheless, O/N_2 is still an indicative parameter for N_mF_2 as we will see in the following analysis.

Figs. 3 and 4 relate trends of h_mF_2 and N_mF_2 to the governing photochemical and transport processes, for solar minimum and solar maximum conditions, respectively. The figures show trends of N_mF_2 and h_mF_2; changes of O/N_2 ratio, and trends of the three plasma transport terms at UT 12:00 near June solstice, under a doubling of CO_2. Since the TIEGCM assumes hydrostatic equilibrium and solves the thermospheric and ionospheric continuity, momentum, and energy equations on pressure surfaces, these changes were calculated on the pressure surfaces where F_2 peak lies.

Trends of N_mF_2 due to the CO_2 cooling effect are negative all over the globe under both solar minimum and solar maximum conditions (Figs. 3a and 4a). Patterns of N_mF_2 trend resemble patterns of O/N_2 changes, especially under solar maximum conditions (Fig. 4a, c). This indicates the important role of O/N_2 in determining N_mF_2. However, even though the changes of O/N_2, both in magnitude and pattern, are similar under solar minimum and solar maximum (Figs. 3c and 4c), the magnitude and pattern of trends of N_mF_2 have a strong dependence on solar activity (Figs. 3a and 4a). Trends of N_mF_2 at solar minimum are more structured and show significant departures from the pattern of change of O/N_2 (Fig. 3a, c). This departure is caused by trends in plasma transport. Figs. 3d–f and 4d–f show trends of the three transport terms: plasma transport by neutral wind, ambipolar diffusion, and $\vec{E} \times \vec{B}$. Under solar minimum conditions, significant modification of photochemical equilibrium by transport processes is clearly seen, and the main contribution is from trends of neutral wind plasma transport (Fig. 3a, d). While pattern and magnitude of trends of N_mF_2 are controlled by trends of O/N_2 under solar maximum conditions, they are significantly modified and controlled by trends of plasma transport processes under solar minimum conditions.

Plasma transport by neutral wind is mainly determined by the meridional wind and vertical gradients of electron density. The meridional wind makes the main contribution to the neutral wind plasma transport since it is in the north–south direction and therefore is largely oriented with the geomagnetic field. The zonal wind also contributes to neutral wind plasma transport especially in some mid-latitude regions where geomagnetic declination angles are large. In order to understand solar cycle variability of the trends of neutral wind plasma transport due to the CO_2 cooling effect, we need to look into the solar cycle variability of

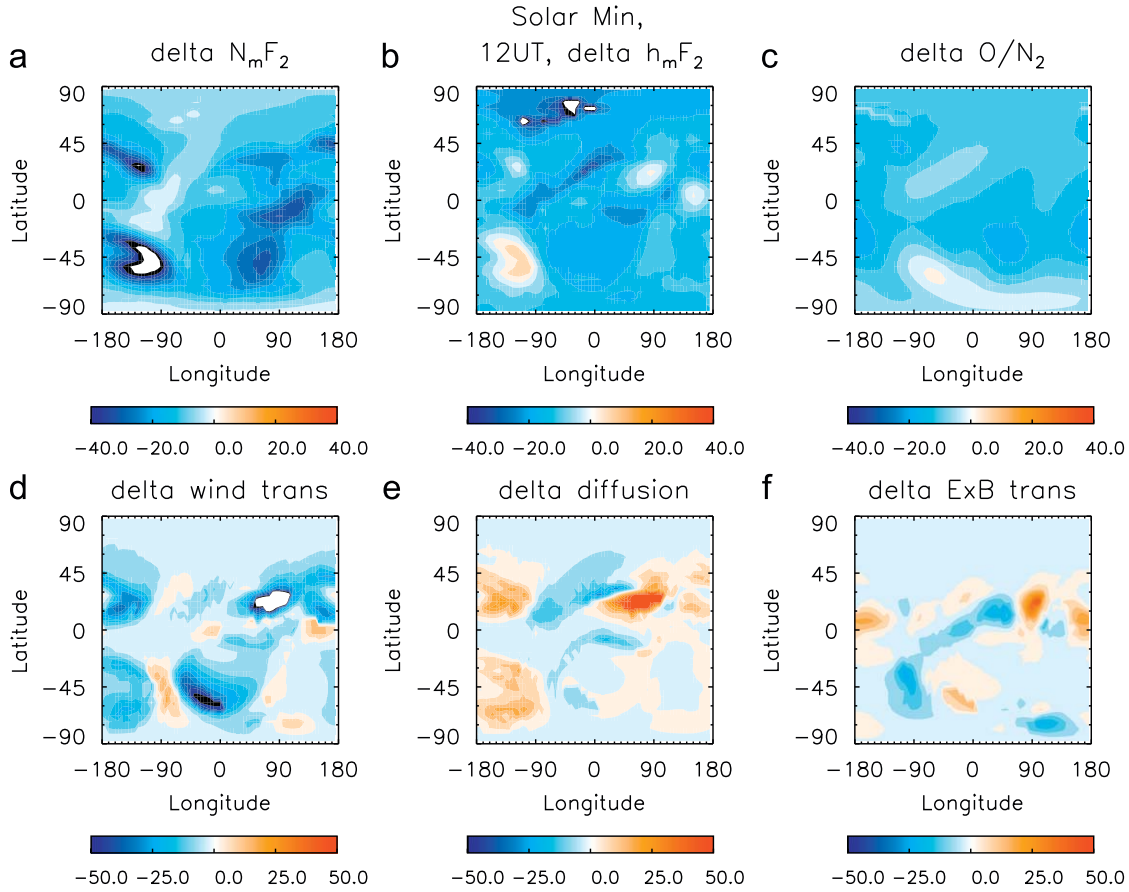

Fig. 3. Changes (double CO_2–base CO_2) of: (a) N_mF_2; (b) h_mF_2; (c) O/N_2; (d) plasma transport by neutral wind; (e) plasma transport by ambipolar diffusion; (f) plasma transport by $E \times B$ drift; under solar minimum conditions at 12:00 UT, assuming geomagnetic quiet condition ($K_p = 1$). The differences are calculated on pressure surfaces where F_2 peaks are located. Values shown in the figures: percentage difference for N_mF_2 and O/N_2; absolute change in km for h_mF_2; and absolute changes in $cm^{-3}\,s^{-1}$ for the three transport terms (Eq. (1)).

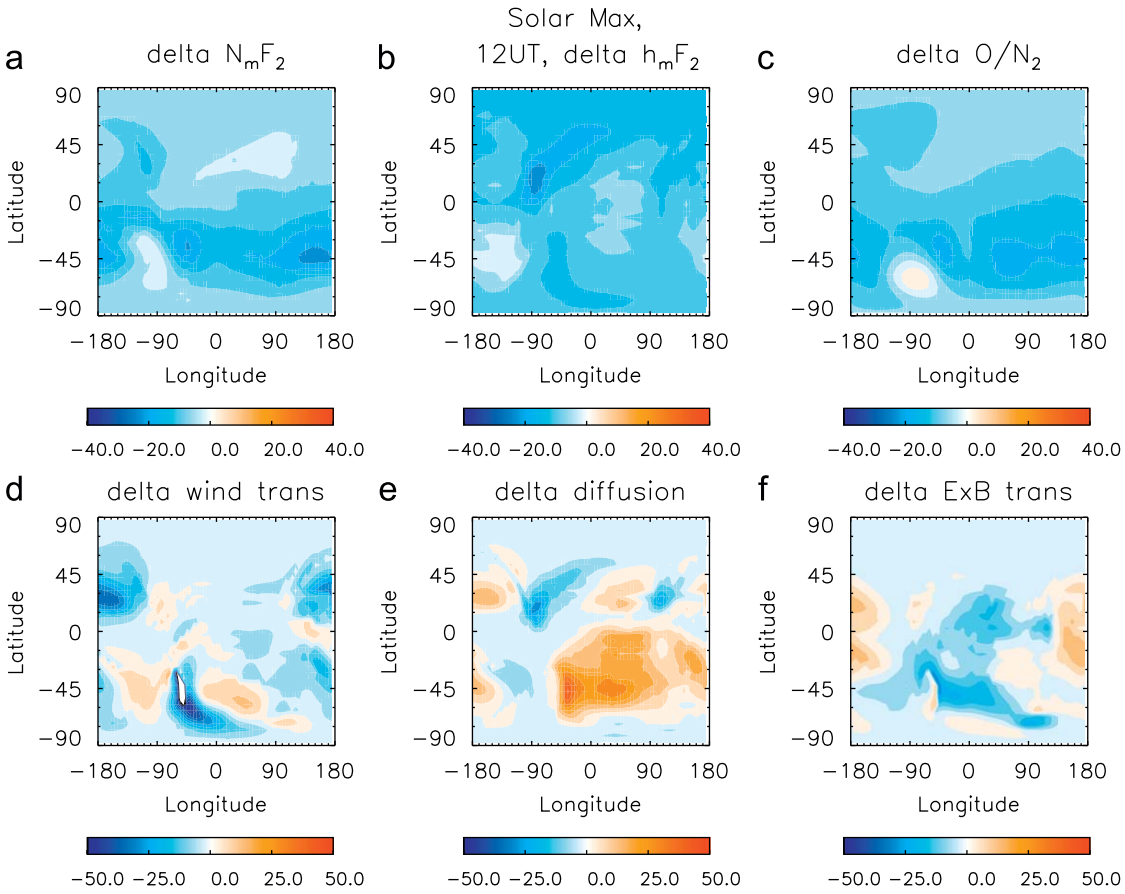

Fig. 4. Changes (double CO_2–base CO_2) of: (a) N_mF_2; (b) h_mF_2; (c) O/N_2; (d) plasma transport by neutral wind; (e) plasma transport by ambipolar diffusion; (f) plasma transport by $E \times B$ drift; under solar maximum conditions at 12:00 UT, assuming geomagnetic quiet condition ($K_p = 1$). The differences are calculated on pressure surfaces where F_2 peaks are located. Values shown in the figures: percentage difference for N_mF_2 and O/N_2; absolute change in km for h_mF_2; and absolute changes in $cm^{-3}\,s^{-1}$ for the three transport terms (Eq. (1)).

trends of neutral wind and the vertical gradient of electron density. Fig. 5 shows changes of the meridional and zonal wind between the CO_2-doubling case and the base case under solar minimum and solar maximum conditions. Patterns of changes of neutral wind are similar at solar minimum and solar maximum, but the magnitude of the change is much larger under solar minimum conditions. In addition, changes of vertical gradients of electron density should also be larger under solar minimum conditions, due to stronger cooling and thus stronger contraction. The greater changes in both neutral wind and the vertical gradient of electron density under solar minimum conditions result in a greater effect of neutral wind plasma transport on N_mF_2 trends. Consequently, neutral wind plasma transport plays a more important role in determining trends of N_mF_2 under solar minimum conditions. Therefore, solar cycle variations of the N_mF_2 trends are mainly caused by solar cycle variations of the response of neutral wind plasma transport to the CO_2 cooling effect at the F_2 peak, due to stronger changes of neutral wind and vertical gradients of electron density under solar minimum conditions.

Figs. 3a and 4a also show that the amplitude of diurnal variations of N_mF_2 trends is generally larger at solar minimum than at solar maximum, and the geographic distribution of N_mF_2 trends is more complex at solar minimum than at solar maximum. These are also caused by the stronger response of neutral wind plasma transport to the greenhouse effect at solar minimum. Changes of neutral wind transport show a larger diurnal amplitude than that of O/N_2, since the trends of N_mF_2 are more modified by the neutral wind transport effect at solar minimum, diurnal variations of the N_mF_2 trend are also more prominent at solar minimum. Since changes of neutral wind transport exhibit a complex geographic structure, the stronger effect of neutral wind transport on N_mF_2 trends increases the complexity of geographic structure of N_mF_2 trends under solar minimum conditions. However, even though changes of O/N_2 show large hemisphere asymmetry under both solar minimum and solar maximum conditions (Figs. 3c, 4c, e.g., changes of O/N_2 are much stronger in the winter hemisphere than the summer hemisphere), changes of neutral wind transport is largely symmetric in term of the total amount in either of the two hemispheres (Fig. 3d). Stronger effects of neutral wind transport on the trend of N_mF_2 neutralizes hemispheric asymmetry of N_mF_2 trends at solar minimum.

Trends of h_mF_2 are negative during the day, but can be positive at night, for both solar minimum and solar maximum conditions. Negative trends of h_mF_2 during the day are on average larger under solar minimum than solar maximum conditions. Rishbeth (1998) found that the F_2 peak tends to remain on the same pressure surfaces as temperature changes. This was verified by the TIEGCM model run that we made. When temperature decreases as a result of increased CO_2 concentration, the F_2 peak remains on the same pressure surface in most cases. Since there is more cooling under solar minimum conditions with the same increase of CO_2 (Emmert et al., 2004; Marcos et al., 2005; Qian et al., 2006), pressure surfaces descend more at solar minimum, and thus stronger negative trends of h_mF_2 occur at solar minimum. In addition, positive trends of h_mF_2 at night are also larger under solar minimum than solar maximum conditions. These positive trends of h_mF_2 are caused by trends of plasma transport. This

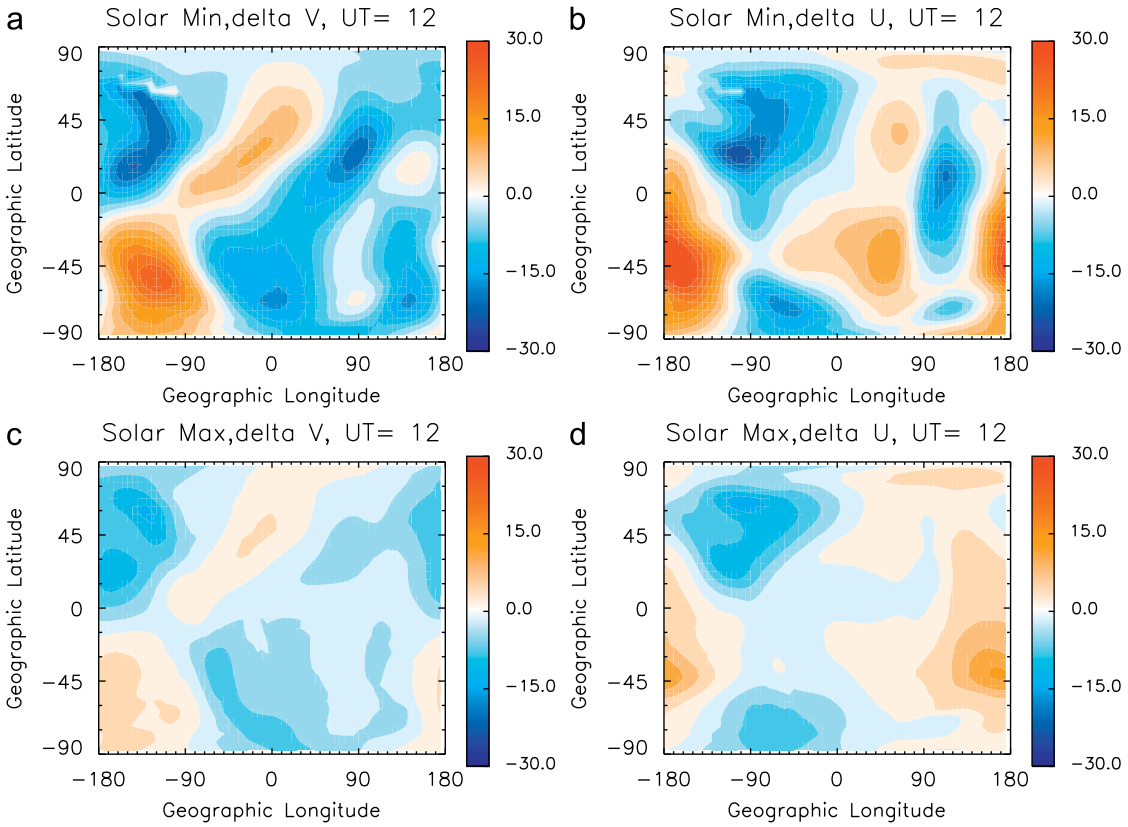

Fig. 5. Changes (double CO_2–base CO_2) of meridional and zonal wind due to cooling and contraction of the thermosphere caused by increased CO_2 concentration, under solar minimum (upper panel) and solar maximum (lower panel) conditions at 12:00 UT, assuming geomagnetic quiet condition ($K_p = 1$). Values shown in the figures are absolution changes in m/s.

transport effect can be demonstrated by examining the longitude sector between −180° and −90° in Figs. 3b, 4b, and 5. The local time for this longitude sector is from midnight to 6:00am. Trends of meridional wind are equatorward in both hemispheres, at both solar minimum and solar maximum. This equatorward trend of the meridional wind has the effect of lifting the F_2 peak to higher pressure surfaces. The trends of zonal wind in this longitude sector also contribute to lift the F_2 peak. The vertical plasma transport velocity due to zonal wind can be expressed as $W = -U \sin I \cos I \sin D$, where U is the zonal wind, I is the geomagnetic inclination angle, and D is the geomagnetic declination angle. In this longitude sector, D is positive in both hemispheres whereas I is positive in the Northern Hemisphere and negative in the Southern Hemisphere. The negative trend of U in the Northern Hemisphere causes a positive W and the positive trend of U in the Southern Hemisphere also causes a positive W. When the effects of lifting are larger than the effects of cooling and contraction, trends of h_mF_2 at these locations become positive. Figs. 3b and 4b show that this is especially true in the winter hemisphere. Furthermore, since the trends of neutral wind are larger under solar minimum conditions, positive trends of h_mF_2 are also larger at solar minimum. Stronger negative trends of h_mF_2 during the day, and larger positive trends at night under solar minimum conditions, also mean that the diurnal amplitude of trends of h_mF_2 is larger under solar minimum conditions than solar maximum conditions.

3.3. *Vertical distribution of trends in the ionosphere*

Previous sections have focused on trends of h_mF_2 and N_mF_2, their dependence on geographic location, local time, season, and solar activity, and analysis of these trends and trend variability. In this section, we will take a look at the vertical distribution of ionospheric trends in the E and F regions. We will choose one longitude from Fig. 1 to look at the vertical distribution of electron density with latitude. Fig. 6a shows the altitude distribution of electron density changes between the CO_2-doubling case and the base case at longitude 0° and local time 12:00 noon. The dotted line in Fig. 6a represents F_2 peak altitude for the base case and the solid line is F_2 peak altitude for the CO_2-doubling case. F_2 peak altitude decreases are approximately in the range of 10–25 km, depending on latitude. Overall, when CO_2 is doubled, electron density increases in the E region and the F region up to near the F_2 peak, above which electron density decreases, with the greatest negative changes occurring above the F_2 peak. This is evident in Fig. 6b. Fig. 6b gives electron density profiles of the base case in red and the CO_2-doubling case in blue for latitude 32°N.

4. Discussion

In Figs. 3 and 4, changes of neutral composition (O/N_2) are plotted to represent its influence on trends of N_mF_2 caused by photochemical production and loss processes; changes of plasma transport caused by neutral wind, ambipolar diffusion, and $\vec{E} \times \vec{B}$ are shown to represent dynamical effects on trends of h_mF_2 and N_mF_2. Both changes of composition and changes of plasma transport show some interesting features.

Changes of O/N_2 exhibit hemispheric/seasonal asymmetry (Figs. 3c and 4c) with much larger O/N_2 changes in the winter hemisphere. Changes of O/N_2 referred to here are changes of O/N_2 on pressure surfaces. The lowering of constant pressure surfaces

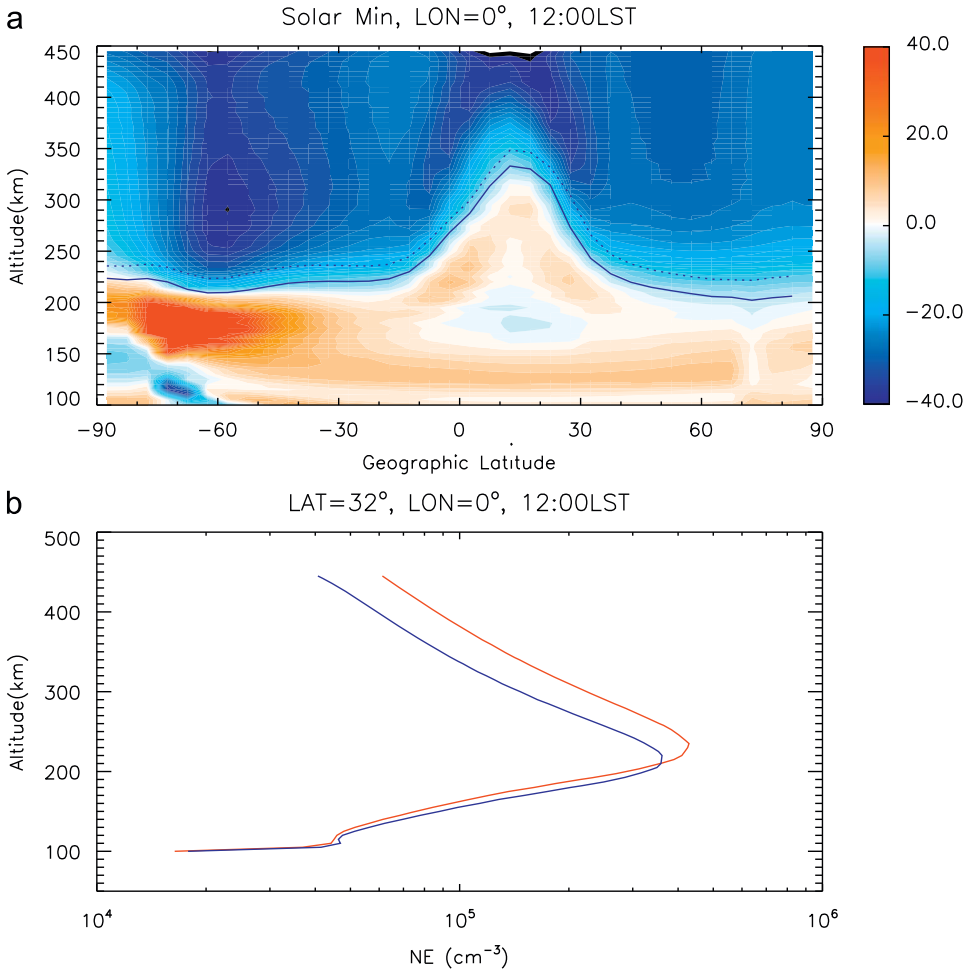

Fig. 6. (a) Changes (double CO_2–base CO_2) of electron density (percentage change) as a function of latitude (*X*-axis) and altitude (*Y*-axis) for one of longitudes of Fig. 1 (longitude = 0°) at local noon, for solar minimum and geomagnetic quiet conditions. Dotted line: F_2 peak for the base CO_2 case; solid line: F_2 peak for the double CO_2 case. (b) Electron density profiles for one of the latitudes of Fig. 6(a) (32°). Red: the base case; blue: the double CO_2 case. (For interpretation of the references to color in this figure legend, the reader is referred to the web version of this article.)

due to cooling and thus thermal contraction does not change the O/N_2 (Rishbeth, 1998). Since the changes of O/N_2 are negative in both of the hemispheres, the changes of O/N_2 shown in Figs. 3c and 4c are likely due to photochemical processes.

Fig. 5 shows that cooling changes the large-scale circulation. Consequently, neutral wind plasma transport also changes due to cooling. Figs. 3 and 4 show that plasma transport by ambipolar diffusion and $\vec{E} \times \vec{B}$ also change due to cooling, but the influence of these two forcing mechanisms on trends is secondary compared to neutral wind plasma transport effects. Figs. 3 and 4 also show that neutral wind plasma transport exhibits significant diurnal and solar cycle variations.

These features of photochemical forcing and transport forcing are reflected in features of trends of h_mF_2 and N_mF_2. Figs. 3 and 4 show that under the CO_2 cooling effect, the percentage changes of N_mF_2 are comparable to percentage changes of neutral composition (O/N_2). This indicates that compositional changes determine the basic magnitudes of trends of N_mF_2. Since compositional changes show strong hemispheric/seasonal asymmetry (Figs. 3c and 4c), trends of N_mF_2 also have strong hemispheric/seasonal asymmetry. Trends of N_mF_2 are much larger in the winter hemisphere. This asymmetry is especially evident under solar maximum conditions (Fig. 4a), when the dynamical effect is weaker (Fig. 5). On the other hand, the dynamical effect, mainly neutral wind plasma transport, can significantly change trends of N_mF_2. Since the dynamical effect has large diurnal and solar cycle variations, it contributes to local time and solar cycle variations of trends of N_mF_2 (Figs. 3 and 4).

Both the trends of h_mF_2 and N_mF_2 show strong solar cycle variations. The mechanisms that cause solar cycle variations of h_mF_2 and N_mF_2 are noteworthy. Thermospheric cooling due to the greenhouse effect is stronger under solar minimum than under solar maximum conditions (Qian et al., 2006), since trends of h_mF_2 involve the lowering of pressure surfaces in most cases, trends of h_mF_2 are larger under solar minimum conditions. In addition, changes of meridional winds, and thus changes that result from dynamical effects, are also stronger under solar minimum conditions. This contributes to additional solar cycle variations of trends of h_mF_2. As mentioned earlier, under the CO_2 cooling effect, percentage changes of N_mF_2 are comparable to those of neutral composition (O/N_2). Figs. 3c and 4c show that compositional changes do not have a significant solar cycle variation; the solar cycle variation of trends of N_mF_2 are mainly due to solar cycle variations of the neutral wind plasma transport effect. Stronger changes of neutral winds under solar minimum conditions contribute to this stronger dynamical effect. In addition, more cooling and contraction at solar minimum also causes more changes in the gradient of the electron density profiles, which can also contribute to the greater change of plasma transport that is caused by neutral winds.

In addition, latitudinal and longitudinal variations of trends of h_mF_2 and N_mF_2 show correlations with the geomagnetic dip equator. This is true for both the daytime (Fig. 1) and nighttime (Fig. 2). This correlation indicates the effect of the Earth's geomagnetic field on these trends. The Earth's geomagnetic field influences plasma transport as the plasma travels along geomagnetic field lines driven by neutral winds. It can also influence plasma transport through $\vec{E} \times \vec{B}$ drifts. Therefore, a secular change in the Earth's geomagnetic field can cause a secular change in h_mF_2 and N_mF_2 (Cnossen and Richmond, 2008).

5. Conclusions

Model simulations were conducted to investigate the CO_2 cooling effect on ionospheric long-term trends, with emphasize on trends of h_mF_2 and N_mF_2. These simulations indicate that greenhouse gas cooling causes contraction of the upper atmosphere and changes of neutral and ion composition in the thermosphere/ionosphere, as well as changes of plasma transport. These changes determine the altitude dependence of ionospheric trends and complex latitudinal, longitudinal, diurnal, seasonal, and solar cycle variations of trends of h_mF_2 and N_mF_2.

Trends of electron density are positive in the E and F regions up to slightly below the F_2 peak, above which trends of electron density become negative.

Percentage changes of N_mF_2 are comparable to percentage changes of neutral composition, indicating important contributions from neutral composition change. However, trends of N_mF_2 are also significantly modified by dynamical influences, mainly through changes of meridional wind and thus neutral wind plasma transport, especially under solar minimum conditions. As well as these general conclusions, the following specific conclusions are made:

1. Under the CO_2 cooling effect, trends of N_mF_2 are negative. Percentage changes of N_mF_2 range from 0% to $\sim$−40% with the doubling of CO_2 depending on location, local time, season, and solar activity. The corresponding trends of h_mF_2 are generally negative as well, with a magnitude from 0 to $\sim$−40 km, also depending on location, local time, season, and solar activity. However, trends of h_mF_2 can be positive, usually after midnight, with a maximum positive trend of $\sim$10 km. These positive trends of h_mF_2 are due to changes in neutral wind plasma transport at these local times, which dynamically increases h_mF_2.
2. Trends of h_mF_2 and N_mF_2 exhibit large latitudinal and longitudinal variations. Both latitudinal and longitudinal distributions of these trends show correlations with the geomagnetic dip equator, indicating the effects of electrodynamics on these trends.
3. Both trends of h_mF_2 and N_mF_2 show strong local time variations and this local time dependence varies with different geographic location. Some locations have larger trends during nighttime while other locations have their largest trends during the day. Trends of h_mF_2 are negative during day time but can be positive at night. In addition, the amplitude of diurnal variations of trends of h_mF_2 and N_mF_2 are larger under solar minimum than solar maximum conditions, due to stronger trends of neutral wind plasma transport at solar minimum.
4. There is a seasonal/hemispheric asymmetry of trends of N_mF_2, with larger trends in the winter hemisphere, which is apparently related to the seasonal/hemispheric asymmetry of neutral composition changes. This hemispheric asymmetry is more evident under solar maximum conditions due to weaker dynamical contributions in this part of the solar cycle.
5. On a global averaged basis, trends of both h_mF_2 and N_mF_2 are larger under solar minimum than solar maximum conditions; and the global distribution of trends tends to be more structured under solar minimum conditions due to the stronger influence of dynamical forcing in this part of the solar cycle. Neutral composition change does not show much solar cycle variation. Solar cycle variations of trends of N_mF_2 is mainly caused by solar cycle variations of trends of plasma transport, with most contributions coming from trends in neutral wind plasma transport, due to the larger trend of neutral wind and the larger change of vertical gradients of electron density under solar minimum conditions.

These conclusions apply to ionospheric trends due to the CO_2 cooling effect. Any secular changes in the upper atmosphere, whether anthropogenic or natural origin, which causes changes in neutral composition, temperature, dynamics, and electrodynamics, should influence ionospheric trends. For example, the ionosphere, especially the F_2 peak, is strongly influenced by geomagnetic storm effects since geomagnetic storms change temperature, composition, dynamics, and electrodynamics. Therefore, trends in geomagnetic activity should be expected to cause trends of h_mF_2 and N_mF_2; secular changes in the geomagnetic poles and thus changes in geomagnetic field can also change electrodynamic coupling between the thermosphere and the ionosphere and thus contribute to ionospheric trends.

Acknowledgements

This research was supported by NASA Grants NNH05AB55I, NNX07AC55G, NNX07AC61G to the National Center for Atmospheric Research (NCAR), and by the Center for Integrated Space Weather Modeling (CISM), which is funded by the STC program under Agreement no. ATM-0120950. NCAR is supported by the National Science Foundation.

Reference

Akmaev, R.A., Fomichev, V.I., 1998. Cooling of the mesosphere and lower thermosphere due to doubling of CO_2. Ann. Geophys. 16, 1501–1512.

Akmaev, R.A., Fomichev, V.I., 2000. A model estimate of cooling in the mesosphere and lower thermosphere due to the CO_2 increase over the last 3–4 decades. Geophys. Res. Lett. 27, 2113–2116.

Akmaev, R.A., Fomichev, V.I., Zhu, X., 2006. Impact of middle-atmospheric composition changes on greenhouse cooling in the upper atmosphere. J. Atmos. Terr. Phys. 68, 1879–1889.

Beig, G., Keckhut, P., Lowe, R.P., Roble, R.G., Mlynczak, M.G., Scheer, J., Fomichev, V.I., Offermann, D., French, W.J.R., Shepherd, M.G., Semenov, A.I., Remsberg, E.E., She, C.Y., Lübken, F.J., Bremer, J., Clemesha, B.R., Stegman, J., Sigernes, F., Fadnavis, S., 2003. Review of mesospheric temperature trends. Rev. Geophys. 41 (4), 1015.

Bremer, J., 1992. Ionospheric trends in mid-latitudes as a possible indicator of the atmospheric greenhouse effect. J. Atmos. Terr. Phys. 54, 1505–1511.

Bremer, J., 1998. Trends in the ionospheric E- and F-regions over Europe. Ann. Geophys. 16, 986–996.

Bremer, J., 2001. Trends in the thermosphere derived from global ionosonde observations. Adv. Space Res. 28, 997–1006.

Bremer, J., Alfonsi, L., Bencze, P., Laštovička, J., Mikhailov, A.V., Rogers, N., 2004. Long-term trends in the ionosphere and upper atmosphere parameters. Ann. Geophys. 47 (Supplement to nos. 2–3), 1009–1029.

Clilverd, M.A., Ulich, T., Jarvis, M.J., 2003. Residual solar cycle influence on trends in ionospheric F2-layer peak height. J. Geophys. Res. 108 (A12), 1450.

Cnossen, I., Richmond, A.D., 2008. Modeling the effects of changes in the Earth's magnetic field from 1957 to 1997 on the ionospheric hmF2 and foF2 parameters. J. Atmos. Terr. Phys. 70, 1512–1524.

Danilov, A.D., Mikhailov, A.V., 1999. Spatial and seasonal variations of foF2 long-term trend. Ann. Geophys. 17, 1239–1243.

Danilov, A.D., 2002. The method of determination of long-term trends in F2-region independent of geomagnetic activity. Ann. Geophys. 20, 1–11.

Danilov, A.D., 2008. Long-term trends in the relation between daytime and nighttime values of foF2. Ann. Geophys. 26, 1199–1206.
Dickinson, R.E., Ridley, E.C., Roble, R.G., 1981. A three-dimensional general circulation model of the thermosphere. J. Geophys. Res. 86, 1499–1512.
Dickinson, R.E., Ridley, E.C., Roble, R.G., 1984. Thermospheric general circulation with coupled dynamics and composition. J. Atmos. Sci. 41, 205–219.
Emmert, J.T., Picone, J.M., Lean, J.L., Knowles, S.H., 2004. Global change in the thermosphere: compelling evidence of a secular decrease in density. J. Geophys. Res. 109, A02301.
Gruzdev, A.N., Brasseur, G.P., 2005. Long-term changes in the mesosphere calculated by a two-dimensional model. J. Geophys. Res. 110, D03304.
Keating, G.M., Tolson, R.H., Bradford, M.S., 2000. Evidence of long-term global decline in the Earth's thermospheric densities apparently related to anthropogenic effects. Geophys. Res. Lett. 27, 1523–1526.
Hagan, M.E., Forbes, J.M., 2002. Migrating and nonmigrating diurnal tides in the middle and upper atmosphere excited by tropospheric latent heat release. J. Geophys. Res. 107 (D24), 4754.
Hagan, M.E., Forbes, J.M., 2003. Migrating and nonmigrating semidiurnal tides in the upper atmosphere excited by tropospheric latent heat release. J. Geophys. Res. 108 (A2), 1062.
Heelis, R.A., Lowell, J.K., Spiro, R.W., 1982. A model of the high-latitude ionospheric convection pattern. J. Geophys. Res. 87, 6339–6345.
IPCC AR4 WG1 report, 2007. Climate Change 2007: The Physical Science Basis.
Laštovička, J., Bremer, J., 2004. An overview of long-term trends in the lower ionosphere below 120 km. Surv. Geophys. 25, 69–99.
Laštovička, J., 2005. On the role of solar and geomagnetic activity in long-term trends in the atmosphere–ionosphere system. J. Atmos. Terr. Phys. 67, 83–92.
Laštovička, J., Akmaev, R.A., Beig, G., Bremer, J., Emmert, J.T., 2006a. Global change in the upper atmosphere. Science 314, 1253–1254.
Laštovička, J., Mikhailov, A.V., Ulich, T., Bremer, J., Elias, A.G., Ortiz de Adler, N., Jara, V., Abarca del Rio, R., Foppiano, A.J., Ovalle, E., Danilov, A.D., 2006b. Long-term trends in foF2: a comparison of various methods. J. Atmos. Terr. Phys. 68, 1854–1870.
Laštovička, J., Akmaev, R.A., Beig, G., Bremer, J., Emmert, J.T., Jacobi, C., Jarvis, M.J., Nedoluha, G., Portnyagin, Y.I., Ulich, T., 2008. Emerging pattern of global change in the upper atmosphere and ionosphere. Ann. Geophys. 26, 1255–1268.
Marcos, F.A., J.Wise, O., Kendra, M.J., Grossbard, N.J., Bowman, B.R., 2005. Detection of a long-term decrease in thermospheric neutral density. Geophys. Res. Lett. 32, L04103.
Mikhailov, A.V., Marin, D., 2000. Geomagnetic control of the foF2 long-term trends. Ann. Geophys. 18, 653–665.
Mikhailov, A.V., Marin, D., 2001. An interpretation of the foF2 and hmF2 long-term trends in the framework of the geomagnetic control concept. Ann. Geophys. 19, 733–748.
Mikhailov, A.V., Marin, D., Leschinskaya, T.Yu., Herraiz, M., 2002. A revised approach to the *fo*F2 long-term trends analysis. Ann. Geophys. 20, 1663–1675.
Mikhailov, A.V., 2006. Ionospheric long-term trends: can the geomagnetic control and the greenhouse hypotheses be reconciled? Ann. Geophys. 24, 2533–2541.
Qian, L., Roble, R.G., Solomon, S.C., Kane, T.J., 2006. Calculated and observed climate change in the thermosphere, and a prediction for solar cycle 24. Geophys. Res. Lett. 33, L23705.
Qian, L., Solomon, S.C., Roble, R.G., Kane, T.J., 2008. Model simulations of global change in the ionosphere. Geophys. Res. Lett. 35, L07811.
Richards, P.G., Fennelly, J.A., Torr, D.G., 1994. EUVAC: a solar EUV flux model for aeronomic calculations. J. Geophys. Res. 99, 8981–8992.
Richmond, A.D., Ridley, E.C., Roble, R.G., 1992. A thermosphere/ionosphere general circulation model with coupled electrodynamics. Geophys. Res. Lett. 19, 601.
Richmond, A.D., 1995. Ionospheric electrodynamics using magnetic apex coordinates. J. Geomagn. Geoelectr. 47, 191–212.
Rishbeth, H., 1990. A greenhouse effect in the ionosphere? Planet. Space Sci. 38, 945–948.
Rishbeth, H., Roble, R.G., 1992. Cooling of the upper atmosphere by enhanced greenhouse gases: modeling of thermospheric and ionospheric effects. Planet. Space Sci. 40, 1011–1026.
Rishbeth, H., 1997. Long-term changes in the ionosphere. Adv. Space Res. 20 (11), 2149–2155.
Rishbeth, H., 1998. How the thermospheric circulation affects the ionospheric F2-layer. J. Atmos. Terr. Phys. 60, 1385–1402.
Roble, R.G., Ridley, E.C., 1987. An auroral model for the NCAR thermosphere general circulation model (TGCM). Ann. Geophys. 5A (6), 369–382.
Roble, R.G., Ridley, E.C., Richmond, A.D., Dickinson, R.E., 1988. A coupled thermosphere/ionosphere general circulation model. Geophys. Res. Lett. 15, 1325.
Roble, R.G., Dickinson, R.E., 1989. How will changes in carbon dioxide and methane modify the mean structure of the mesosphere and thermosphere? Geophys. Res. Lett. 16, 1144–1441.
Xu, Z.-W., Wu, J., Igarashi, K., Kato, H., Wu, Z.-S., 2004. Long-term ionospheric trends based on ground-based ionosonde observations at Kokubunji, Japan. J. Geophys. Res. 109, A09307.